Check for updates

ORIGINAL ARTICLE

Reactivation of hydrated cement powder by thermal treatment for partial replacement of ordinary portland cement

Gustave Semugaza (iD) · **Tommy Mielke** · **Marianela Escobar Castillo** ·
Anne Zora Gierth · **Joo Xian Tam** · **Stefan Nawrath** · **Doru C. Lupascu**

Abstract Cement is the strength-forming component of concrete. It has been a major building material for more than a century. However, its production is accountable for a considerable percentage of global CO_2 emissions and is very energy-intensive. The Ordinary Portland Cement (OPC) production is a thermal process at around 1450 °C. This study shows that the reactivation of Hydrated Cement Powder (HCP) can be successful at a much lower temperature. Therefore, the possibility of using HCP to replace parts of OPC in concrete reduces the energy consumption and the CO_2 emissions associated with OPC production. HCP, which may ultimately stem from recycled concrete, needs treatment to produce new concrete of the required mechanical strength. Using reactivated HCP in concrete, an optimum strength is achieved by heating the HCP in the range of 400–800 °C. Among other factors, the type of cement used influences the optimum heating temperature and attainable strength. This paper shows that 600 °C is an optimum heating temperature using the OPC type CEM I 52.5R. The crystalline phase transitions resulting from the thermal treatment were analyzed by X-ray diffraction (XRD), differential scanning calorimetry (DSC), and thermogravimetry (TG). The heat released during hydration was investigated, and scanning electron microscopy (SEM) displays the microstructure evolution. OPC can be partially replaced by thermally treated HCP in mortar, attaining similar mechanical strength values.

Keywords Hydrated cement powder · Dehydrated cement powder · Thermal treatment · Reactivation · Partial replacement of ordinary portland cement · Mechanical performance

G. Semugaza (✉) · T. Mielke · M.
E. Castillo · A. Z. Gierth · J. X. Tam ·
S. Nawrath · D. C. Lupascu
Institute for Materials Science and Center for Nanointegration Duisburg-Essen (CENIDE), Faculty of Engineering, University of Duisburg-Essen, 45141 Essen, Germany
e-mail: gustave.semugaza@stud.uni-duisburg-essen.de

1 Introduction

Cement is the major binder of concrete and mortars. Its use has become omnipresent for around a century, the first usage dating back a few millenniums. Despite its massive impact on the environment, there is an increasing demand for concrete [1–4]. Cement production today is accountable for about 7% of global CO_2 emissions. The mineral source of calcium ions is calcium carbonate generating two-thirds of these CO_2 emissions during decomposition. The subsequent formation of clinker phases in a furnace at 1450 °C

rilem

is very energy-intensive, generating another third of the CO_2 emissions [5, 6]. Ongoing demolition and large amounts of concrete fines that have been landfilled as waste constitute a potential for reducing emissions by recycling cementitious parts [7–9]. The reactivation of Hydrated Cement Powder (HCP) is possible at much lower temperatures than those required for the production of ordinary Portland Cement (OPC), reducing the overall energy consumption [10].

The strength achieved for the reactivated material is lower than those of OPC, but this material can already be used to replace parts of the OPC in new concrete production [10, 11]. Laboratory-produced materials have been compared with directly used old concrete [12, 13] or with OPC [14, 15]. The five stages of hydration are commonly known, but since the processes are highly complex, research continues to identify which chemical processes take place during hydration in detail. The temperature rise due to hydration is faster the finer the cement grinding due to increased specific surface area [16].

HCP can recover its hydration capacity by being exposed to temperatures between 400 and 900 °C [17, 18]. Some hydration products are progressively dehydrated at elevated temperatures, including ettringite $[Ca_6(Al(OH)_6)_2(SO_4)_3(H_2O)_{26}]$, Calcium Silicate Hydrates (C–S–H) and portlandite, $[Ca(OH)_2]$, abbreviated as 'CH' [12, 19–22]. Previous research has reported that dehydration can recover these products for renewed use. Rehydration is the reaction of Dehydrated Cement Powder (DCP) with water [13, 23–25]. Different chemical processes occur during dehydration in different temperature ranges [10, 17, 24, 26–29]. At a temperature of 105 °C, evaporable water from pores or cavities and parts of the physically bound water are liberated. Water is completely eliminated at 120 °C. The ettringite decomposition occurs between 110 and 170 °C. Some anhydrous cement phases, including larnite (C_2S) and brownmillerite (C_4AF), exist in the latter temperature range. Portlandite decomposition happens in the temperature range of 400–550 °C, and lastly, calcite ($CaCO_3$) decomposes between 600 and 900 °C.

The ability to bind water is regained by rehydrating the DCP but with a set of different properties. The higher the dehydration temperature, the higher the water demand for standard consistency. That is due to a higher Blaine surface area and the immediate reaction of dehydration products such as free CaO and ettringite that drive up the water demand. Correlating with the higher water demand is a decreasing setting time [23]. Research on the heat flow during rehydration has shown that the curves of DCP have a similar shape as OPC showing induction, acceleration, and deceleration periods. While the peak of heat flow for OCP is at the end of the acceleration period, DCP offers a higher initial heat. This also depends on the dehydration temperature: the higher the dehydration temperature, the higher the initial heat. As stated above, the high surface area drives the initial temperature rise. The instability of the dehydration products and the high CaO concentration of DCP can be further reasons therefore [30].

The reactivation potential can be quantified by the regained cement strength. Shui et al. [23] found that the compressive and flexural strengths were maximum with a treatment at 800 °C and decreased with thermal treatment above 800 °C. Alternatively, Real et al. [30] found the highest strength to be achieved for cement dehydrated at 650 °C. A significant relationship exists between the chemical transformations by thermal treatment and the achievable compressive and flexural strengths [31].

We here performed an extensive investigation of the phase transitions induced by thermal treatment of HCP determining the optimum strength development temperature range along with phase analysis by Rietveld refinement. The variety of methods confirms the results of previous studies and establish a clear association between the obtained strength and the dehydration temperature. CEM I 52.5 R had not been considered in the research field so far. It is comparatively reactive similar to the retreated cement, and can thus offer a route to develop future treatment strategies for cement powders.

2 Materials and methods

2.1 Materials and sample preparation

The OPC type CEM I 52.5 R Wittekind (from Erwitte town in Germany) was used in the experiments. First, Hydrated Cement Specimens (HCS) were made from the mixture of OPC and water (w/c = 0.5). After curing for 28 days, Hydrated Cement Powder (HCP) was produced by crushing and grinding HCS. The

HCP was then sieved to the grain size < 250 μm. Finally, Dehydrated Cement Powder (DCP) was obtained after thermal treatment of HCP at different temperatures from 200 to 1000 °C. The CEN standard sand conforming to ISO 679 (Beckum/Germany) was used for mortar production. The mortar mix ratio was selected according to DIN EN 196-1, with (450 ± 2) g of OPC, HCP, DCP or a mixture; (1350 ± 5) g of sand; and (225 ± 1) g of water. Figure 1 summarizes the process applied to produce the materials used.

2.2 Preparation of dehydrated cement powders (DCP)

The Hydrated Cement Specimens (HCS) were prepared in prismatic steel molds 40 × 40 × 160 mm³ and left in the molds for 24 h in containers keeping the humidity inside. They were then cured in water for 6 days and for another 21 days in the temperature control room (at ± 20 °C and ± 65% RH) according to DIN EN 12390-2. Part 2: Making and curing specimens for strength tests; German version EN 12390-2:2019. After curing, the HCS were crushed with a jaw crusher and ground milled (Retzsch) to obtain HCP of grain size < 250 μm after sieving. The HCP was then heated in batches in a muffle furnace (Nabertherm) at temperatures from 200 to 1000 °C, with a heating rate of 5 °C/min, 1 h hold time at maximum temperature and naturally cooled to room temperature to obtain the DCP. The HCP and DCP were stored in sealed buckets or small sealed glass containers to avoid carbonation. Figure 1c illustrates the heating regime of the HCP.

2.3 X-Ray diffraction (XRD) and scanning electron microscope (SEM)

XRD was used to identify the main crystalline phases using an Empyrean powder diffractometer (PANalytical) with Cu K$_\alpha$ radiation over a 2-theta range of 5°–
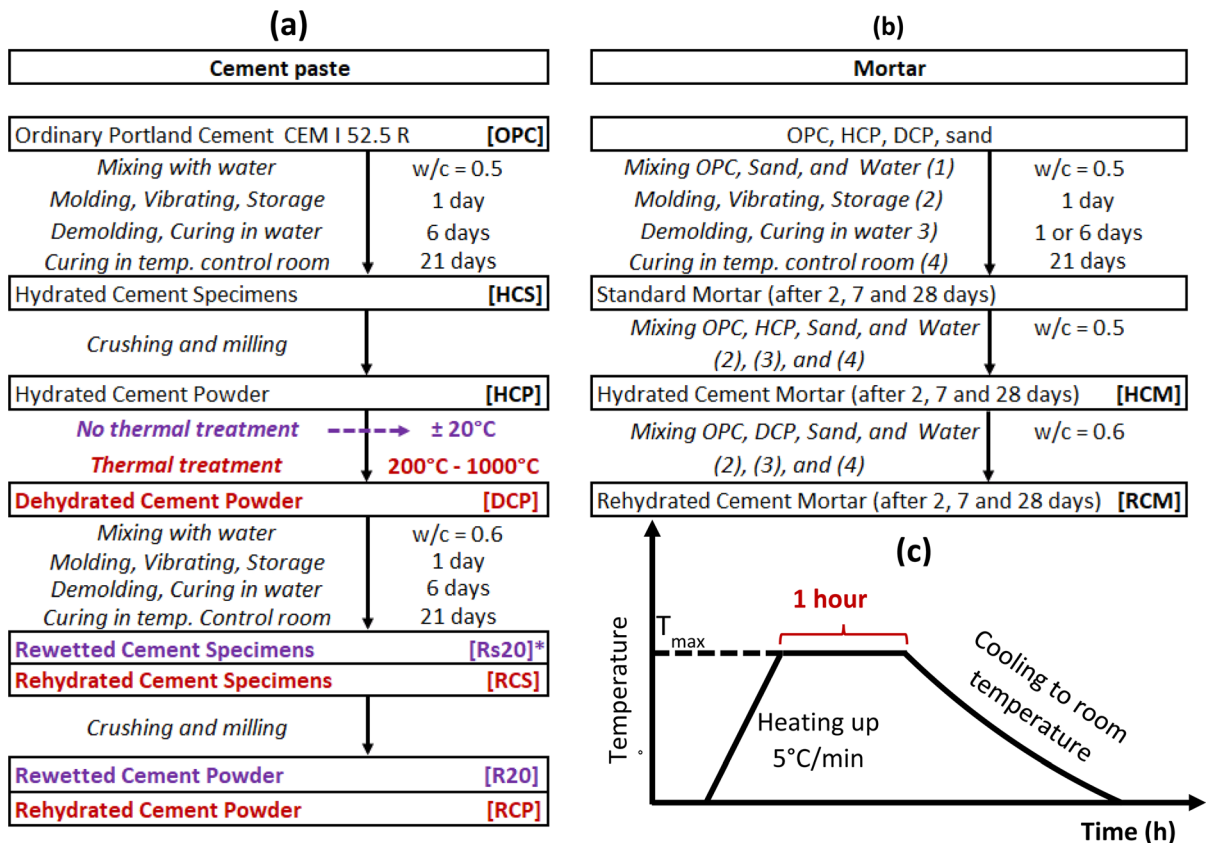

Fig. 1 The process applied for material preparation. **a** Cement paste, **b** Mortar, **c** Heating regime used for HCP. Rs20* = specimens obtained by mixing HCP (not thermally treated) with water

90° (step size of 0.013°, scan speed 0.018°/s). The High Score Plus program was used to assess the crystalline phases. An SEM was used to investigate the microstructure evolution between the HCS and the Rehydrated Cement Specimens (RCS) made from DCP after treatment at different temperatures. The samples were coated using a Sputter Coater Cressington MTM 10 (Au80Pd20 target). For the elemental analysis in the SEM, EDX (Energy Dispersive X-ray Spectroscopy, energy resolution < 129 eV for Mn K radiation, detector surface 100 mm^2) point analysis was used. The SEM/EDX samples were obtained from the specimens (HCS and RCS) previously used for the compressive strength tests. The samples were stored in a desiccator under vacuum to avoid carbonation.

2.4 Differential scanning calorimetry (DSC) and thermogravimetry (TG)

DSC was used to identify the heat flow in and out of the HCP and DCP. TG measurements were used to determine the weight losses related to the peaks. The DSC–TG measurements were conducted concurrently in a NETZSCH STA 449F1 Jupiter with a silicon carbide oven, in the temperature range from 25 to 1000 °C at 10 K/min heating and cooling rates.

2.5 Reaction heat release

The heat released during the hydration of OPC and rehydration of HCP and DCP was used to assess the reactivity of the materials. The setup is shown in Fig. 2.
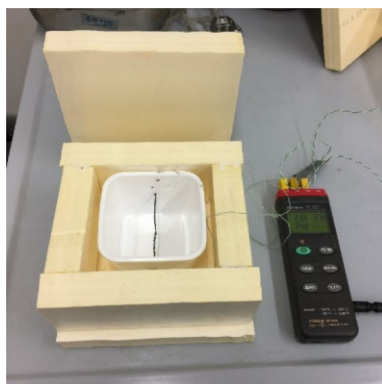
Fig. 2 Experimental setup for the determination of the heat release during the hydration of OPC and rehydration of HCP and DCP

A styrofoam container with a thickness of 3 cm was assembled for insulation. A thin plastic container (approx. $86 \times 86 \times 86$ mm) was used as mold for the water/cement mixture containing a thermocouple in its center, recording the temperature every 20 s over 3 days. The temperature of the room was measured in parallel to exclude errors. The same *w/c* ratio was used as in strength testing. The samples were always weighed before the experiment to ensure the same mass.

2.6 Specific surface area

The specific surface areas of OPC and DCP were determined with the air permeability method (Blaine method) according to the German standard DIN EN 196-6:2018.

2.7 Porosity

The porosity was evaluated on the HCS and the RCS by mercury intrusion porosimetry (MIP) with a maximum test pressure of 400 MPa, mercury surface tension of 0.48 N/m, and mercury contact angle of 140°. The samples were obtained from the remaining specimens (HCS and RCS) previously used for the compressive strength test. When possible, the samples were taken from the center, about 3–4 g. The samples were stored under vacuum inside the MIP device for approximately 20 min before the measurement started to ensure they were free of moisture. Forceps, a small hammer and tweezers were used to prepare the required sample size ($\sim 1 \times 1 \times 1 \text{cm}^3$) and mass ($\sim 1.6$–2.0 g) for measurement.

2.8 Compressive and flexural strengths

The compressive and flexural strengths were evaluated on mortar using 100% OPC, or replaced with DCP (10, 20, 30, and 100%). In the case of 100% replacement of OCP with DCP, the superplasticizer (2% by mass of DCP), MC-PowerFlow 1102 (MC Bauchemie, Bottrop, Germany), was necessary to control the setting time and regulate the hydration process. The OPC was used to make the Standard Mortar, the HCP was used to make the Hydrated Cement Mortar (HCM). The DCPs, after treatment at different temperatures, provided the Rehydrated Cement Mortars (RCM). The mortar mix ratio was selected according to DIN EN

196-1 (equivalent to the European Standard EN 196-1), with (450 ± 2) g of OPC, HCP, DCP or mixtures; (1350 ± 5) g of sand; and (225 ± 1) g of water. A prismatic steel mold $40 \times 40 \times 160$ mm^3 was used to make the specimens. The compressive and flexural strengths were measured after 2, 7, and 28 days following curing for 1 day in the mold, 6 days in water, and 21 days in the temperature control room (at ± 20 °C and $\pm 65\%$ RH). The three-point bending method was used to measure the flexural strength resulting in two pieces subsequently used for compressive strength testing.

3 Results and discussion

3.1 Crystalline phases and microstructure of rehydration products

Figure 3a and b illustrate the XRD patterns of the dehydrated and rehydrated cement powders after treatment at different temperatures. HCP serves as a reference containing the main crystalline phases such as portlandite $[Ca(OH)_2]$, ettringite $[Ca_6(Al(OH)_6)_2(SO_4)_3(H_2O)_{26}]$, dicalcium silicate $[Ca_2SiO_4, C_2S]$ and tobermorite (C–S–H) $[Ca_5Si_6O_{16}(OH)_2]$, see Table 1 for phase percentages. No ettringite phase was identified in any of the dehydrated samples (D200 to

D1000). This non-existence of ettringite specifies that it decomposes below 200 °C during heating [32, 33]. The reappearance of the ettringite phase in rehydrated samples prepared by mixing water with DCP (R200 to R800) and cooled down to room temperature, indicates that this process is reversible due to the reaction of the DCP phases with water (Fig. 3b).

Figure 3a displays a decrease in portlandite peak intensities above D400. The calcite phase tends to disappear above D600, revealing the decomposition of portlandite and calcite above 400 and 600 °C via dehydroxylation $(Ca(OH)_2 \rightarrow CaO + H_2O)$ and decarbonation $(CaCO_3 \rightarrow CaO + CO_2)$, respectively. This free lime should be avoided, so carbonation of the raw recycling product should be avoided as much as possible. Table 1 shows that the thermal treatment of HCP at 200 °C (D200) and 400 °C (D400) provides very similar phase content. Generally, increasing the content of the C_2S and C_3S phases enhances the strength development in the mortar [14]. In the rehydrated samples (Fig. 3b), R600 has a higher percentage of tricalcium silicate than R20, R200, R400, and R800. The R20 strength development results from the non-reacted fraction of HCP, which allows for a minor rebinding ability. Although the R1000 has a high content of dicalcium silicates, it contains very low tricalcium silicates affecting the total strength development, especially in the early
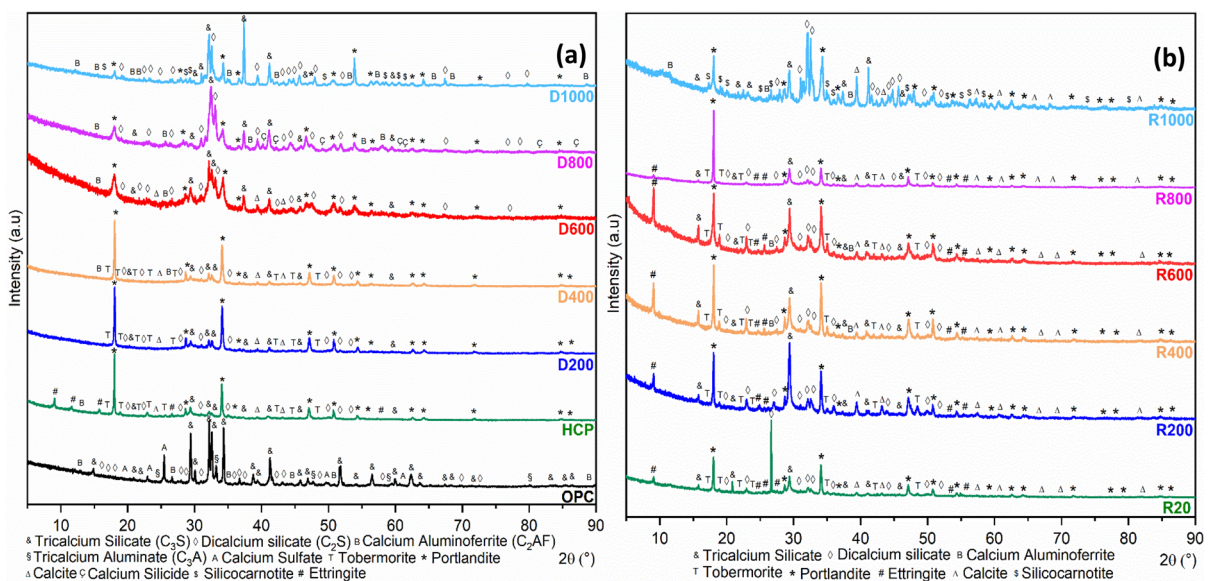
Fig. 3 XRD patterns of **a** dehydrated cement powder obtained after thermal treatment at different temperatures. **b** Shows the XRD diffractograms of these powders after the reaction with water at room temperature

Table 1 Phase content from XRD spectra after Rietveld refinement ($\pm$ 0.5%)

Phase	Untreated		Dehydrated					Rehydrated					
	OPC	HCP	D200	D400	D600	D800	D1000	R20	R200	R400	R600	R800	R1000
Ettringite [$Ca_6Al_2(SO_4)_3(OH)_{12} \cdot 26H_2O$]		15%						9%	7%	15%	13%	4%	14%
Portlandite [$Ca(OH)_2$]		30%	34%	34%	22%	12%	2.5%	22%	14%	19%	18%	25%	62%
Dicalcium Silicate [Ca_2SiO_4]	18%	12%	20%	21%	50%	73%	82%	15%	16%	11%	13%	22%	
Tricalcium Silicate [Ca_3SiO_5]	73%	1.5%	6%	5%	24%	10%	0.5%	1%	2%	3%	6%	2%	0.5%
Calcium Aluminoferrite [$Ca_2(Al,Fe)_2O_5$]	1%	0.5%		1%	1%	4%	5%			4%	3%		1.5%
Tricalcium Aluminate [$Ca_3Al_2O_6$]	4%												
Calcium Sulfate [$CaSO_4$]	4%												
Tobermorite (C–S–H) [$Ca_5Si_6O_{16}(OH)_2$]		34%	38%	36%				41%	33%	35%	31%	20%	
Calcite [$CaCO_3$]		7%	2%	3%	3%			12%	28%	13%	16%	27%	8%
Silicocarnotite [$Ca_5Si_2SO_{12}$]						1%	10%						14%
Calcium Silicide [$CaSi_2$]													

stage. The current research considered 28 days cured primary material, while the completion of water–cement reaction takes up to many years.

The XRD peaks associated with thermal treatment at 1000 °C (D1000 & R1000) are dissimilar to the treatments at lower temperatures yielding a high percentage of new phases (14% Silicocarnotite [Ca_5-Si_2SO_{12}]), and no C–S–H forms with rehydration. These new phases as well as the more difficult workability of the rehydrated cement paste, negatively affect the strength development of this batch [10, 23]. Therefore, the optimum range of material strength development is between 400 and 800 °C. D600 provides the highest tricalcium silicate content, which is responsible for early strength development [34].

Figure 4 shows the SEM and EDX images of HCS (a), rewetted (b) and rehydrated cement specimens (c, d, e, f, g, and h) obtained after dehydration at different temperatures (from 200 to 1000 °C). The HCS (Fig. 4a) is a reference for the other samples. Hydration (HCS) and rehydration (RCS) products, such as ettringite, can be observed. According to the EDX point analysis, this phase is identified as needles in the microstructure. The plate-like features represent the portlandite phase, while the little broken shapes represent the dicalcium or tricalcium silicate phases. XRD analysis reveals that the ettringite phase disappears with thermal treatment above 200 °C. However, after the samples have been cooled down to room temperature and rehydrated, the ettringite phase reappears. This reappearance does not happen with thermal treatment at 1000 °C.

From SEM images we can see the following steps during the rehydration process. First, no significant changes happen. The ettringite phase grows from untreated (Rs20) (Fig. 4b) to Rs400 (Fig. 4d). Next, with thermal treatment at 600 °C (Rs600) (Fig. 4e), no more growth of the ettringite phase happens. The ettringite phase content decreases with this treatment temperature, and more calcium silicate phases are formed. This behavior results in a densified and more compact structure, leading to increased strength development. Next, the thermal treatment at 800 °C (Rs800) (Fig. 4f) yields a highly reactive material which does not allow for consistent workability of the rehydrated products, yielding heterogeneous microstructures and thus lower strength values. Lastly, as indicated by the XRD results, the ettringite and C–S–H phases completely disappear with thermal

treatment at 1000 °C (Rs1000) (Fig. 4g), and new crystalline phases arise. This behavior indicates an alteration of already dehydrated hydration products [23, 35], negatively affecting strength as well. EDX point analysis reveals the intensity of chemical elements contained per point analyzed. The chemical compositions of the phases can be found in Table 1 (XRD phase content). Combining the XRD and SEM/EDX gives insight on the optimum heat treatment. However, strength development of the pre-heated HCP has to be verified to complete the story.

3.2 Specific surface area of the powders and heat release during hydration

The specific surface area of the OPC and DCP increases with thermal treatment, except for 1000 °C (Fig. 5a). The dehydrated cement powders result from crushing and milling the hydrated cement specimens from the OPC mixed with water. Thus, there is thus an alteration of the OPC particles and, therefore, a change in the specific surface area. Different transformations and decompositions resulting from thermal treatment cause differences between the specific surface areas of the DCPs depending on the temperature used. The thermal treatment generates the dehydration of the C–S–H gels and ettringite decomposition below 250 °C, the dehydroxylation between 400 and 550 °C, and the decarbonation between 600 and 900 °C. The DSC results (Sect. 3.3) show these transformations. Nevertheless, the specific surface area decreases from D400 to D1000. This might be caused by the agglomeration of particles due to the high temperatures. The agglomeration phenomenon is more prominent on D1000 than on the other DCPs [30].

Figure 5b illustrates the heat release during the hydration of OPC and rehydration of HCP and DCP. The dehydration temperature influences the chemical composition of DCP and the rehydration activity. The higher the dehydration temperature, the higher the initial heat release indicating high initial reactivity in the first minutes of rehydration. We analyzed the temperature of the total system, i.e. the developed heat released within the sample.

The temperature curves are very different according to the individual chemical composition. Except for HCP, the temperature development at the beginning of hydration is similar but strikingly much higher for D800 and D1000, reaching more than ten times the
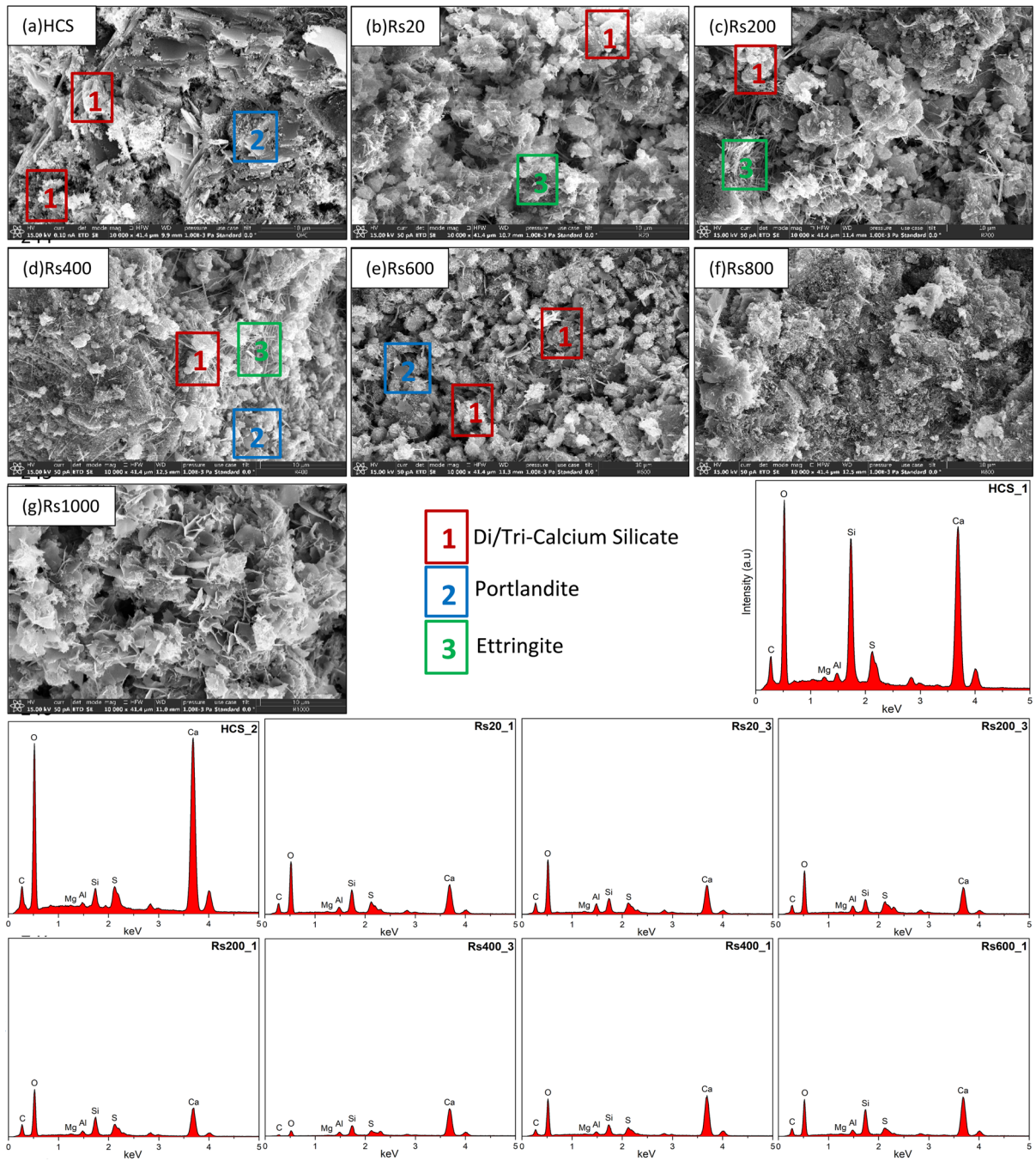
Fig. 4 SEM and EDX images of **a** hydrated cement specimen, **b** rewetted cement specimen (no thermal treatment) and **c–g** rehydrated cement specimens (after thermal treatment). The EDX images indicate the intensity of chemical elements contained per point analyzed

one of OPC. The hydration levels of OPC are well known [36–42]. Therefore, the measured temperature curve of OPC corresponds to the generally known stages of hydration. An increase in temperature can be seen in the first minutes after mixing with water. Subsequently, it stagnates for about 2 h. This corresponds to the initial reaction followed by the induction period. Within about 10 h, the temperature of the
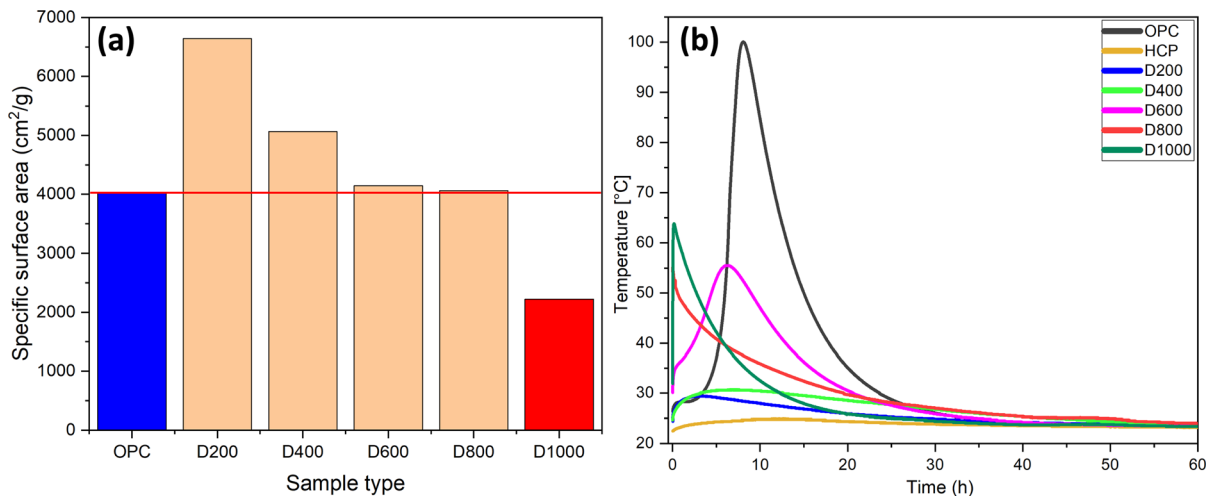
Fig. 5 **a** Comparison of the specific surface area of OPC and dehydrated cement powders (DCP); **b** the temperature rise during the hydration of OPC, the rehydration of untreated HCP, and the rehydration of thermally treated HCP

system rises to just above 100 °C. Afterwards, the heat generated is lower than the heat leaving the system, so the temperature decreases. That part can be assigned to the acceleration and deceleration periods. The HCP reacts with water without considerable heat release because it was already hydrated before mixing. The reaction of the remaining anhydrous compounds does not have a viewable influence on the hydration heat [30, 42, 43]. Within the first 10 h of the reaction, the temperature of the cement paste merely increases by 2–3 °C.

D200 and D400 have similarly high heat releases of about 30 °C in the first minutes of the reaction. While the temperature of the D200 paste decreases quite rapidly before the first 30 min have elapsed, the temperature of the D400 paste still rises just above 30 degrees and drops after about 7 h. Within the first 3 h, the temperature curve is higher for D200 and D400 than for OPC, indicating a more significant initial reaction. The temperature curves of the rehydration of D800 and D1000 are characterized by the cement paste developing a very high temperature in the first minutes. The temperature then decreases without further peaks. D800 reaches about 55 °C, D1000 rises to almost 65 °C. Subsequently, the reactions peter out as both temperature curves decelerate sharply. After about 6 h, the curves cross due to a steeper temperature drop for D1000. This increased initial heat release can result from the high surface area, the

instability of the dehydration products, and the high CaO concentration of DCP (Real et al. [30]).

The shape of the temperature curve of the D600 pastes is closest to that of OPC. In the first minutes of rehydration, the temperature is about 7 °C warmer than for OPC. Stagnation is not evident, and the temperature rise occurs correspondingly earlier. The maximum temperature of 55 °C, nearly half that of OPC paste, is reached earlier than for OPC. Compared to OPC, the initial heat release of D600 is much higher. However, the acceleration peak is reached earlier because the periods are shorter. The smaller peak compared to OPC suggests that full reactivity cannot be restored with just a thermal treatment of 600 °C. Nevertheless, recognizing all hydration stages, especially the acceleration and deceleration periods, corresponds to the highest strength development. Different authors have stated that portlandite crystals grow into the interstices of the clinker grains during the acceleration period [44–47]. The C–S–H forms around the silicate clinker surfaces and successively grows into the pore solution. This bridges spaces, which increases the viscosity of the cement paste. Solidification is reached when the intergranular voids are fully bridged. In addition, during the deceleration period, the remaining pore spaces are filled with C–S–H, which densifies the microstructure. This section specifies that the hydration of the HCP pre-treated at 600 °C behaves closest to the hydration of OPC compared to the other pre-treatment temperatures.
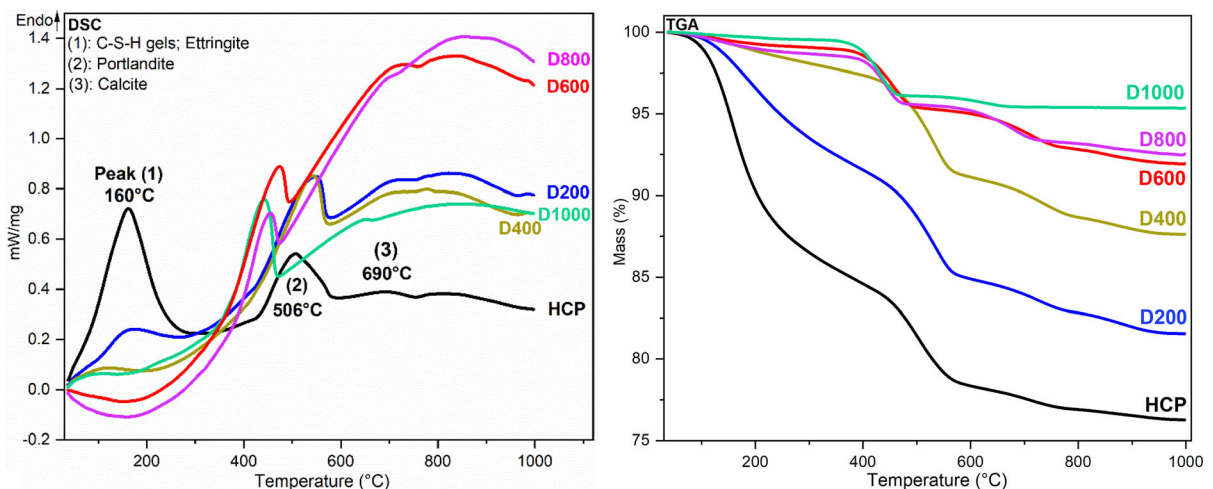
3.3 Identification of phase transitions

Figure 6 compares the DSC (mW/mg) and TG (% mass loss) curves of hydrated cement powder (HCP) and dehydrated cement powders (D200 to D1000) at a constant heating rate. Three prominent peaks are identified. Several authors [26, 48–50] have indicated the ranges for these peaks and explained their causes. The first peak at 160 °C is due to water loss, mainly from the dehydration of the C–S–H gels and ettringite decomposition. The second peak identified at 506 °C is due to the dehydroxylation of portlandite, while the third peak at 690 °C results from the decarbonation of calcite. These peaks are connected to principal weight losses. The first loss happens between 125 and 195 °C, the second between 470 and 550 °C, and the third between 640 and 750 °C (± 10 °C).

In the DSC curve, the samples pre-heated at 400–1000 °C do not present the first peak, namely low or no mass losses (TG curve) in this range. The TG curve of D200 shows that the mass loss ranges approximately from 117 to 242 °C; thus, the dehydration of C–S–H gels and decomposition of ettringite are complete in this temperature range which agrees with the literature stating 250 °C [24]. On the other hand, the second DSC peak at around 506 °C remains even for the samples pre-heated above 600 °C. Considering that the dehydroxylation reaction of portlandite is completed with pre-treatment below 600 °C, it can be concluded that portlandite was not completely decomposed in all samples. These results agree with the XRD phase analysis (Table 1). However, this second peak shifts to lower temperatures in the samples D600, D800, and D100. Therefore, the recrystallized phase is not as thermally stable as the original portlandite from the OPC.

Considering the decarbonation reaction, the results show that the third peak is identified in all samples but tends to disappear for the samples pre-heated at 800 and 1000 °C. There has been more decomposition liberating CO_2 associated with the thermal pre-treatment at these temperatures, causing a decrease in the calcite phase content. Sabeur et al. [51] have stated that the new quantities of CaO produced by the decomposition of calcite and portlandite combine, but a decrease in calcite mass is noted for thermal treatment above 600 °C. At a temperature around 800 °C, a non-pronounced fourth peak is identified in all samples. However, in some samples (D400, D800, D1000), the third and fourth peaks cannot be well distinguished. This fourth peak is associated with very low or no mass loss. Therefore, it is related to a phase transformation assigned to the recrystallization of possible remaining calcite [30]. The contribution of these decompositions to the strength development was discussed in Sect. 3.1.

Fig. 6 Comparison of DSC (mW/mg) and TG (% mass loss) curves of hydrated cement powder (HCP) and dehydrated cement powders (D200 to D1000)
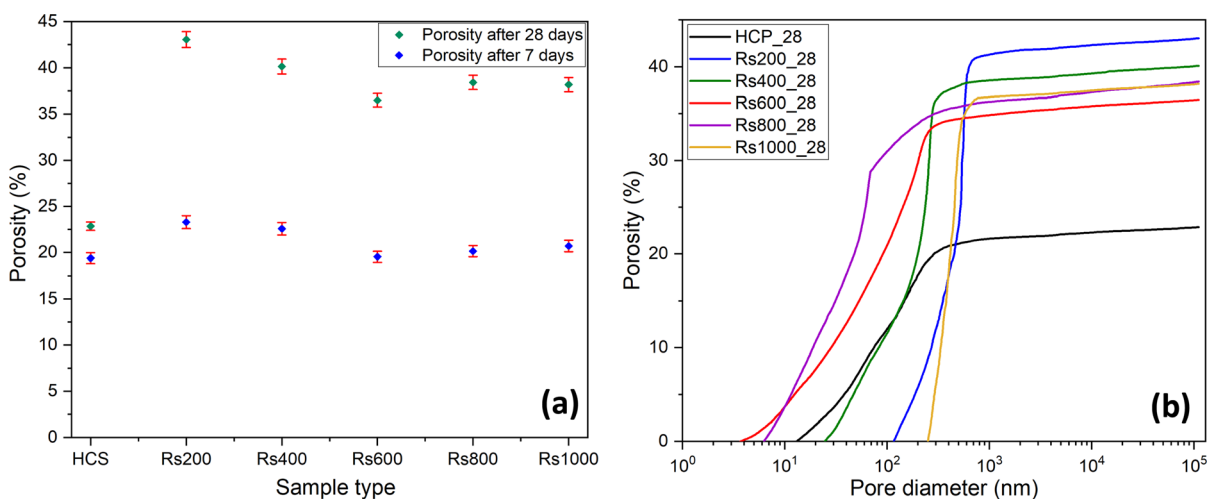
3.4 Porosity

Figure 7a shows the mercury intrusion porosity of the HCS and RCS (Rs200–Rs1000). It increases from 7 to 28 days between the same sample types. Presumably, the porosity after 7 days was highly affected by the residual water remaining in small pores even after storage under vacuum inside the device before porosity measurement. The MIP results display much higher inaccessible porosity (22–41%) on specimens cured for 7 days compared to 28 days.

The continuous water loss through drying out results in capillary pores, and the hydration reactions initiate the smaller gel pores. The porosity formation rate is very high for the rehydrated specimens because the hydration reactions are very rapid. Pores form inside the material because the fresh paste loses the opportunity to densify in a medium viscosity regime. Therefore, it will be necessary to use chemical additives to control the setting time in the future.

The porosity evolution due to heat treatment can be explained by combining the DSC (for phase transformations) and XRD (for phase contents) results. The Rs200 forms higher porosity than HCS after removing the physically bound water from the C–S–H gel and ettringite decomposition [52, 53]. The porosity is similar between Rs200 and Rs400 as no significant decomposition of the hydration products occurs. There is coexistence of portlandite and calcite [26, 28]. In the case of Rs400 to Rs600, the porosity decreases due to the decomposition of portlandite, offering the CaO. The last regime arises between Rs600 and Rs1000. The decomposition of calcite, a tiny peak, liberates a small amount of CaO, and the contents in calcium silicate phases are similar. The pore structure does not change much; therefore, the porosity results are alike in this temperature range.

After 7 days, the porosity of all samples is similar because there is considerable water content, and the hydration reaction is still happening to a great extent. Besides, the high inaccessible porosity during the measurement of specimens cured for 7 days is also to be considered here. However, after 28 days, we observe that the specimen Rs200 has higher porosity. This could be due to the lower content of calcium silicates (Table 1) compared to the other specimens. On the other hand, the Rs600 after 28 days tends to show the lowest porosity specifying the highest degree of compactness and the least amount of void space, indicating an optimum thermal treatment at 600 °C with respect to setting dynamics of the rehydrated cement. Additionally, Fig. 7b shows that Rs600_28 has the lowest cumulative pore diameter of all thermally treated samples, with a median pore diameter of 76 nm, and shifts most to the lower values of pore diameters. This emphasizes the potential for optimum strength development with thermal treatment at 600 °C.

Fig. 7 **a** Comparison of porosity of the HCS and RCS manufactured from the HCP thermally treated at different temperatures as indicated. **b** Cumulative pore size distribution after 28 days
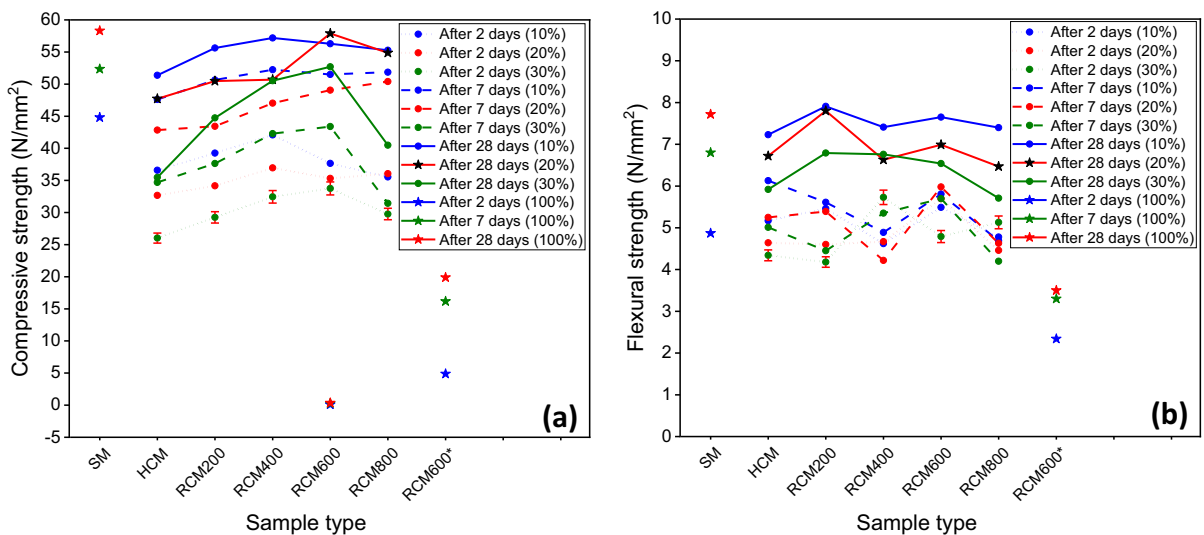
3.5 Compressive and flexural strengths of rehydrated cement mortar

Ultimately, cement is part of a mortar or concrete. In order to evaluate whether binding to the sand fraction changes due to the different heat treatments, we also investigated a set of mortars from the produced cement mixtures. The influence of DCP on the mortar strength was evaluated by replacing the OPC with different percentages of DCP (10, 20, 30, and 100%). For comparison, we also prepared the specimens with 100% OPC. Three types of mortar were prepared, including the standard mortar (using OPC), the hydrated cement mortar "HCM" (using HCP), and the rehydrated cement mortar "RCM" (using DCP). We used CEM I 52.5 R cement as the binder to prepare the standard mortar. Different dehydration temperatures were considered (from 200 to 800 °C), and the complete influence of the optimum heating temperature (100% D600) was assessed. Figure 8a and b shows the compressive and flexural strengths after curing for 2, 7 and 28 days.

Generally, the compressive strength decreases as the proportion of OPC replacement increases for all curing times. Also, the compressive strength increases with curing time for the same dehydration temperature as expected, Fig. 8a. The rehydrated cement mortar, RCM 600, with 20% OPC replacement, shows the best results compared to the standard mortar. It achieves

99.3% of the compressive strength of the SM. As the dehydration temperature increases further, an abrupt drop occurs for RCM 800. Therefore, the dehydration temperature plays a vital role in the rehydration behavior and strength recovery. This strength decrease results from the transformation of already dehydrated hydration products. For example, Alonso and Fernandes [24] reported that the C–S–H gel transforms to a newly formed nesosilicate phase above 750 °C, causing a strength decrease.

Considering the substitution by 30% of D600, the strength decreases significantly, indicating that OPC can only be partially replaced by up to 20% without significantly affecting the mechanical performance. Since 600 °C is the best dehydration temperature, we have assessed 100% replacement of OPC with D600. However, the preparation of specimens using 100% D600 was difficult. The hydration reaction and hardening were too fast. The rapid setting induces high porosity, which in turn reduces strength. Thus, the strengths of these specimens were very low (Fig. 8a). The use of a superplasticizer became necessary. The hydration reaction is retarded with the help of a superplasticizer leading to reduced porosity and higher strength. The strength of 100% RCM 600 after 28 days achieves 34% of the compressive strength of standard mortar and 45% of the flexural strength. These results show that some hydration ability is recovered, but the binding capacity

Fig. 8 Comparison of **a** compressive and **b** flexural strengths of standard mortar (SM), hydrated cement mortar (HCM) and rehydrated cement mortar (RCM), with different replacement percentages of OPC by HCM or RCM. The error bars are representative of all points. RCM600_100* means that the specimens were prepared using a superplasticizer (2%)

is lower than for OPC, even using a superplasticizer. More investigation is needed for a detailed assessment of the resulting microstructure to understand whether the intrinsic strength decreases or just too many large pores are generated during curing, yielding the lowered strength values.

The flexural strength results do not present any specific trend (Fig. 8b). The strength does not always increase with curing time for the same dehydration temperature. The thermal treatment temperature has a minor influence on the strength development. The presence of pores less affects the flexural strength than compressive strength, but increases scatter. In a compression test, the entire sample is under load, and the whole set of internal flaws is tested, namely the entire Weibull distribution. In flexural testing, only a small portion of the sample is under load. Therefore, the statistical scatter is larger, and there is effectively no clear trend in our set of flexural data. Nevertheless, the flexural strength tends to decrease as the replacement of OPC with DCP increases. A remarkable drop is observed on RCM 800 after 7 and 28 days (Fig. 8b). As previously specified, this unpredicted trend is due to induced cracks that affect the internal structure of the specimens. Chen et al. [54] found that the ratio between the compressive and flexural strengths of the cement mortar depends on porosity. Moreover, a study by Piasta et al. [55] on the changes in the structure of hardened cement paste due to high temperature specifies a non-linear change in the distribution of pore diameters and total porosity. Vysvaril et al. [56] indicate that the porosity increases in a non-linear way as the dehydration temperature increases, influencing the flexural and partly the compressive strength.

4 Conclusions

The main objective of this research was to investigate the rehydration ability of hydrated cement powder through thermal treatment at different temperatures. A highly reactive cement type (CEM I 52.5 R) was used to evaluate the highest possible strength recovery through the reactivation method. A partial replacement of OPC by DCP in mortar mixes was assessed with respect to mechanical strength. The following conclusions can be drawn:

(1) Thermal treatment is a valuable method for the reactivation of HCP. Through this method, the HCP converts to DCP containing the strength development phases, mainly the calcium silicates. This thermal treatment recovers some hydration ability, with potential to develop strength. Many similarities are found between the crystalline phases of the OPC and the HCP treated in the range of 400–800 °C. The HCP treated at 600 °C develops the highest strength. It contains the highest amount of tricalcium silicate responsible for early and total strength development. The heat release analysis during hydration confirms the close similarities in the shape of the temperature curves of the D600 and the OPC pastes. The dissimilarity and formation of new crystalline phases in the HCP treated at 1000 °C imply the transformation of already dehydrated hydration phases. Thus, the strength development is negatively affected by very high temperature treatment.

(2) The dehydration reaction of C–S–H gels and decomposition of ettringite are complete below 250°, while the decomposition of portlandite is not complete for all pre-treatment temperatures. Since the latter reaction peak shifts to lower temperatures with pre-treatment above 400 °C, the recrystallized phase is not as thermally stable as the original portlandite from the OPC. The tendency of decarbonation reaction to disappear with pre-treatment above 600 °C can be related to more expulsion of CO_2 from the residual calcite decomposition.

(3) The compressive strength decreases as the proportion of OPC replacement increases for the rehydrated cement mortar. The RCM 600 with 20% OPC replacement (80/20 RCM 600) was optimal, achieving 99.3% of the compressive strength of the SM. OPC can be partially replaced by DCP up to 20% without impairing mechanical performance. The degree of OPC replacement can be increased in case of a low strength requirement.

(4) The assessment of the total replacement of OPC with DCP for the optimum dehydration temperature (100% RCM 600) shows that some hydration ability can be recovered, but the binding capacity is low. Only 34% of the compressive strength of SM and 45% of the

flexural strength are achieved. This lower binding ability can be attributed to a minor percentage or no tricalcium silicate phase, which is the main phase contributing to the strength development.

(5) The porosity increases with curing time (from 7 to 28 days) for the hydrated and rehydrated cement specimens due to the continuously drying water loss and hydration, which results in capillary and gel pores. Therefore, the porosity increase is higher for the rehydrated cement specimens, and the use of chemical additives is needed to control the setting time. Among the thermally treated samples, Rs600 shows the lowest porosity. SEM and EDX point analysis display more calcium silicate phase content resulting in the densification of the rehydration products and a more compact structure. The highly inaccessible porosity during the measurement of porosity after 7 days due to residual pore water explains the lower observed values compared to 28 days of curing.

Declarations

References

1. Imbabi MS, Carrigan C, McKenna S (2012) Trends and developments in green cement and concrete technology. Int J Sustain Built Environ 1(2):194–216. https://doi.org/10.1016/j.ijsbe.2013.05.001

2. Adesina A (2020) Recent advances in the concrete industry to reduce its carbon dioxide emissions. Environ Challenges 1:100004. https://doi.org/10.1016/j.envc.2020.100004

3. Collivignarelli MC, Cillari G, Ricciardi P et al (2020) The production of sustainable concrete with the use of alternative aggregates: a review. Sustainability 12(19):7903. https://doi.org/10.3390/su12197903

4. Javadabadi MT, Kristiansen DDL, Redie MB et al. (2019) Sustainable concrete: a review. IJSCER, pp 126–132. https://doi.org/10.18178/ijscer.8.2.126-132

5. Malhotra VM (2000) Role of supplementary cementing materials in reducing greenhouse gas emissions. In: Gjorv OE, Sakai K (eds) Concrete technology for a sustainable development in the 21st century, vol 226, p 35.

6. He Z, Zhu X, Wang J et al (2019) Comparison of CO2 emissions from OPC and recycled cement production. Constr Build Mater 211:965–973. https://doi.org/10.1016/j.conbuildmat.2019.03.289

7. Alexandru T, Marinela B, Laura D et al (2019) Mechanical and environmental performances of concrete using recycled materials. Proc Manufact 32:253–258. https://doi.org/10.1016/j.promfg.2019.02.211

8. Gebremariam AT, Di Maio F, Vahidi A et al (2020) Innovative technologies for recycling End-of-Life concrete waste in the built environment. Resour Conserv Recycling 163: 104911. https://doi.org/10.1016/j.resconrec.2020.104911

9. Nikmehr B, Al-Ameri R (2022) A state-of-the-art review on the incorporation of recycled concrete aggregates in geopolymer concrete. Recycling 7(4):51. https://doi.org/10.3390/recycling7040051

10. Florea MVA, Ning Z, Brouwers HJH (2014) Activation of liberated concrete fines and their application in mortars.

Constr Build Mater 50:1–12. https://doi.org/10.1016/j.conbuildmat.2013.09.012

11. Xinwei M, Zhaoxiang H, Xueying L (2010) Reactivity of dehydrated cement paste from waste concrete subjected to heat treatment. In: Second international conference on sustainable construction materials and technologies

12. Sui Y, Ou C, Liu S et al (2020) Study on properties of waste concrete powder by thermal treatment and application in mortar. Appl Sci 10(3):998. https://doi.org/10.3390/app10030998

13. Xuan DX, Shui ZH (2011) Rehydration activity of hydrated cement paste exposed to high temperature. Fire Mater 35(7):481–490. https://doi.org/10.1002/fam.1067

14. Kurdowski W (2014) Cement and concrete chemistry. Springer, New York

15. Locher FW (2006) Cement: principles of production and use. Verlag Bau+ Technik GmbH, Düsseldorf

16. Hu J, Ge Z, Wang K (2014) Influence of cement fineness and water-to-cement ratio on mortar early-age heat of hydration and set times. Constr Build Mater 50:657–663. https://doi.org/10.1016/j.conbuildmat.2013.10.011

17. Castellote M, Alonso C, Andrade C et al (2004) Composition and microstructural changes of cement pastes upon heating, as studied by neutron diffraction. Cem Concr Res 34(9):1633–1644. https://doi.org/10.1016/S0008-8846(03)00229-1

18. Handoo SK, Agarwal S, Agarwal SK (2002) Physico-chemical, mineralogical, and morphological characteristics of concrete exposed to elevated temperatures. Cem Concr Res 32(7):1009–1018. https://doi.org/10.1016/S0008-8846(01)00736-0

19. Yu R, Shui Z (2013) Influence of agglomeration of a recycled cement additive on the hydration and microstructure development of cement based materials. Constr Build Mater 49:841–851. https://doi.org/10.1016/j.conbuildmat.2013.09.004

20. Qu B, Fernández Jiménez A, Palomo A et al (2020) Effect of high temperatures on the mechanical behaviour of hybrid cement. Mater construcc 70(337):213. https://doi.org/10.3989/mc.2020.13318

21. Song H, Jeong Y, Bae S et al (2018) A study of thermal decomposition of phases in cementitious systems using HT-XRD and TG. Constr Build Mater 169:648–661. https://doi.org/10.1016/j.conbuildmat.2018.03.001

22. Tantawy MA (2017) Effect of high temperatures on the microstructure of cement paste. MSCE 05(11):33–48. https://doi.org/10.4236/msce.2017.511004

23. Shui Z, Xuan D, Chen W et al (2009) Cementitious characteristics of hydrated cement paste subjected to various dehydration temperatures. Constr Build Mater 23(1):531–537. https://doi.org/10.1016/j.conbuildmat.2007.10.016

24. Alonso C, Fernandez L (2004) Dehydration and rehydration processes of cement paste exposed to high temperature environments. J Mater Sci 39(9):3015–3024. https://doi.org/10.1023/B:JMSC.0000025827.65956.18

25. Carriço A, Bogas JA, Guedes M (2020) Thermoactivated cementitious materials—a review. Constr Build Mater 250:118873. https://doi.org/10.1016/j.conbuildmat.2020.118873

26. Alarcon-Ruiz L, Platret G, Massieu E et al (2005) The use of thermal analysis in assessing the effect of temperature on a cement paste. Cem Concr Res 35(3):609–613. https://doi.org/10.1016/j.cemconres.2004.06.015

27. Farage M, Sercombe J, Gallé C (2003) Rehydration and microstructure of cement paste after heating at temperatures up to 300 °C. Cem Concr Res 33(7):1047–1056. https://doi.org/10.1016/S0008-8846(03)00005-X

28. Stepkowska ET, Blanes JM, Franco F et al (2004) Phase transformation on heating of an aged cement paste. Thermochim Acta 420(1–2):79–87. https://doi.org/10.1016/j.tca.2003.11.057

29. Yu R, Shui Z, Dong J (2011) Activation of fly ash with dehydrated cement paste. ACI Mater J 108(2):204–208

30. Real S, Carriço A, Bogas JA et al (2020) Influence of the treatment temperature on the microstructure and hydration behavior of thermoactivated recycled cement. Materials (Basel, Switzerland) 13(18):3937. https://doi.org/10.3390/ma13183937

31. Bordy A, Younsi A, Aggoun S et al (2017) Cement substitution by a recycled cement paste fine: role of the residual anhydrous clinker. Constr Build Mater 132:1–8. https://doi.org/10.1016/j.conbuildmat.2016.11.080

32. Guimarães D, Oliveira VA, Leão VA (2016) Kinetic and thermal decomposition of ettringite synthesized from aqueous solutions. J Therm Anal Calorim 124(3):1679–1689. https://doi.org/10.1007/s10973-016-5259-3

33. Jiang C, Fang J, Chen J-Y et al. (2020) Modeling the instantaneous phase composition of cement pastes under elevated temperatures. Cement Concrete Res 130:105987. https://doi.org/10.1016/j.cemconres.2020.105987

34. Li Z (2011) Advanced concrete technology. Wiley, Hoboken N.J.

35. Wang G, Zhang C, Zhang B et al (2015) Study on the high-temperature behavior and rehydration characteristics of hardened cement paste. Fire Mater 39(8):741–750. https://doi.org/10.1002/fam.2269

36. Novotný R, Bartoníčková E, Švec J et al (2016) Influence of active alumina on the hydration process of portland cement. Proc Eng 151:80–86. https://doi.org/10.1016/j.proeng.2016.07.383

37. Linderoth O, Wadsö L, Jansen D (2021) Long-term cement hydration studies with isothermal calorimetry. Cement Concrete Res 141: 106344. https://doi.org/10.1016/j.cemconres.2020.106344

38. Briendl LG, Mittermayr F, Röck R et al. (2022) The hydration of fast setting spray binder versus (aluminum sulfate) accelerated OPC. Mater Struct 55(2). https://doi.org/10.1617/s11527-022-01907-x

39. Boháč M, Palou M, Novotný R et al (2014) Investigation on early hydration of ternary Portland cement-blast-furnace slag–metakaolin blends. Constr Build Mater 64:333–341. https://doi.org/10.1016/j.conbuildmat.2014.04.018

40. Maheswaran S, Kalaiselvam S, Palani GS et al (2016) Investigations on the early hydration properties of synthesized β-belites blended cement pastes. J Therm Anal Calorim 125(1):53–64. https://doi.org/10.1007/s10973-016-5386-x

41. Yao W, Guo B, Yang Z et al. (2021) Research on curing water demand of cementing material system based on hydration characteristics. Materials (Basel, Switzerland) 14(22). https://doi.org/10.3390/ma14227098

42. Schmid M, Pichler C, Lackner R (2019) Engineering hydration model for ordinary Portland cement based on heat flow calorimetry data. J Therm Anal Calorim 138(3):2283–2288. https://doi.org/10.1007/s10973-019-08165-0

43. Pang X, Bentz DP, Meyer C et al (2013) A comparison study of Portland cement hydration kinetics as measured by chemical shrinkage and isothermal calorimetry. Cement Concr Compos 39:23–32. https://doi.org/10.1016/j.cemconcomp.2013.03.007

44. Kiernożycki W, Błyszko J (2021) The Influence of Temperature on the Hydration Rate of Cements Based on Calorimetric Measurements. Materials (Basel, Switzerland) 14(11). https://doi.org/10.3390/ma14113025

45. Rahhal V, Talero R (2005) Early hydration of portland cement with crystalline mineral additions. Cem Concr Res 35(7):1285–1291. https://doi.org/10.1016/j.cemconres.2004.12.001

46. Wilińska I, Pacewska B, Antonovič V (2022) Hydration processes of four-component binders containing a low amount of cement. Materials (Basel, Switzerland) 15(6). https://doi.org/10.3390/ma15062192

47. Bligh MW, d'Eurydice MN, Lloyd RR et al (2016) Investigation of early hydration dynamics and microstructural development in ordinary Portland cement using 1H NMR relaxometry and isothermal calorimetry. Cem Concr Res 83:131–139. https://doi.org/10.1016/j.cemconres.2016.01.007

48. Maddalena R, Hall C, Hamilton A (2019) Effect of silica particle size on the formation of calcium silicate hydrate [C-S-H] using thermal analysis. Thermochim Acta 672:142–149. https://doi.org/10.1016/j.tca.2018.09.003

49. Pavlík Z, Trník A, Kulovaná T et al (2016) DSC and TG analysis of a blended binder based on waste ceramic powder and portland cement. Int J Thermophys 37(3):32. https://doi.org/10.1007/s10765-016-2043-3

50. Alexandre Bogas J, Carriço A, Real S (2022) Thermoactivated recycled cement. In: M. Saleh H (ed) Sustainability of concrete with synthetic and recycled aggregates. IntechOpen

51. Sabeur H, Saillio M, Vincent J (2019) Thermal stability and microstructural changes in 5 years aged cement paste subjected to high temperature plateaus up to 1000 °C as studied by thermal analysis and X-ray diffraction. Heat Mass Transfer 55(9):2483–2501. https://doi.org/10.1007/s00231-019-02599-w

52. Prochoń P, Piotrowski T (2016) Bound water content measurement in cement pastes by stoichiometric and gravimetric analyses. J Build Chem 1:18–25

53. Pereira MC, Soares A, Flores-Colen I et al (2020) Influence of exposure to elevated temperatures on the physical and mechanical properties of cementitious thermal mortars. Appl Sci 10(6):2200. https://doi.org/10.3390/app10062200

54. Chen X, Wu S, Zhou J (2013) Influence of porosity on compressive and tensile strength of cement mortar. Constr Build Mater 40:869–874. https://doi.org/10.1016/j.conbuildmat.2012.11.072

55. Piasta J, Sawicz Z, RudzjDski L (1984) Changes in the structure of hardened cement paste due to high temperature. Matériaux et Construction 17:291–296

56. Vyšvařil M, Bayer P, Chromá M et al (2014) Physico-mechanical and microstructural properties of rehydrated blended cement pastes. Constr Build Mater 54:413–420. https://doi.org/10.1016/j.conbuildmat.2013.12.021